

**Drought-Induced Warming in the Continental United States
Under Different SST Regimes**

Randal D. Koster, Hailan Wang¹, Siegfried D. Schubert,
Max J. Suarez, and Sarith Mahanama¹

Global Modeling and Assimilation Office NASA/GSFC, Greenbelt, MD 20771

¹Also at UMBC/GEST, Baltimore, MD

Submitted to Journal of Climate

(Special Issue on US-CLIVAR Drought Working Group Experiments)

February 3, 2009

Abstract

The U.S. CLIVAR Drought Working Group (DWG) recently performed a series of experiments in which a number of AGCMs were forced with different leading patterns of global SST variability. These experiments provide a unique opportunity to examine how different SST regimes affect temperature over the continental United States. We focus here on a particular aspect of June-August (JJA) near-surface air temperature: the temperature during relatively dry years for a given SST regime. For most of the models participating in the DWG experiments, a cold Pacific produces greater warming in the central U.S. during relatively dry years than does a warm Pacific for two separate reasons: (i) the cold Pacific leads, on average across all years, to drier conditions, and (ii) the particular evaporation regime induced by the cold Pacific enhances the impact of evaporation feedback on temperature, i.e., the sensitivity of temperature to within-climate variations in moisture availability. These results are supported, to a large extent, by the observational record.

1. Introduction

Anomalously dry periods are sometimes associated with anomalously warm periods, especially when considering summertime averages (Namias 1960; Chang and Wallace 1987, Karl 1986; Huang et al., 1996; Durre et al. 2000; Shinoda and Yamaguchi 2003). The connection is through evaporation – drier soils can produce reduced evaporation and thus a reduced evaporative cooling of the land surface, which in turn leads to higher temperatures. The higher temperatures associated with dry conditions (hereafter referred to loosely as “drought-induced warming”) can lead to increased crop stress and increased overall energy demand, exacerbating the dry period’s economic impact.

A recent study (Koster et al., 2009a; hereafter K09) examined drought-induced warming in the context of an underlying functional relationship between soil moisture and evaporation. A highly idealized version of this relationship, long discussed in the literature (e.g., Budyko 1974; Manabe 1969; Eagleson 1978), is illustrated in Figure 1. The x-axis represents soil moisture, expressed here as degree of saturation. The y-axis represents the ratio of evaporation to net radiation, i.e., the evaporative fraction, EF. (For this ratio, evaporation is expressed in terms of latent heat flux from the surface, so that EF is dimensionless.) The plot suggests two distinct regimes of evaporation sensitivity to soil moisture. At lower soil moisture levels, an increase in soil moisture implies an increase in evaporation. At higher levels, the sensitivity disappears, and the evaporative fraction remains constant. Hydrologists sometimes refer, somewhat imprecisely, to these two regimes as the “soil moisture-controlled” and “energy-controlled” evaporation regimes. In the latter, wetter regime, transport of moisture through the soil matrix and

vegetation is relatively efficient and no longer acts as a bottleneck to the net transfer of water from the soil to the atmosphere.

K09, recognizing the aforementioned connection between seasonally-averaged evaporation and surface temperature, used the curve in Figure 1 to interpret interannual variations in June-August (JJA) temperature averages in terms of the two evaporation regimes. They showed, using both atmospheric general circulation model (AGCM) data and multi-decadal precipitation and temperature observations, that drier-than-average JJA conditions in regions characterized by soil moisture-controlled evaporation do indeed lead to positive seasonal temperature anomalies, whereas drier-than-average conditions in regions with energy-controlled evaporation do not. Simply put, drought-induced warming tends to occur in some regions but not in others, for straightforward reasons. The AGCM and observational results show strong geographical similarity both in this first-order behavior and in some more subtle second-order diagnostics, suggesting that the AGCM realistically captures the soil-wetness / evaporation / temperature connections operating in nature.

Recently, USCLIVAR (the United States contribution to the World Climate Research Programme's Climate Variability Study) put together a Drought Working Group (DWG) tasked, among other things, with using AGCMs to quantify the impacts of different sea surface temperature (SST) distributions on North American drought. The different AGCM groups comprising the DWG performed the same coordinated series of numerical simulations, each simulation in the series utilizing a different idealized SST distribution. Schubert et al. (this special issue) describe the DWG experiments in detail.

A key result (Schubert et al., this issue) of the DWG experiments is that different SST patterns do tend to generate different precipitation regimes over North America. Accordingly, different SST patterns have the potential to shift a region's operating evaporation regime from soil moisture-controlled to energy-controlled, or vice-versa, with consequent effects on the feedback of evaporation on temperature – i.e., on the potential for drought-induced warming. Indeed, the DWG experiments provide a unique opportunity to determine how different SST patterns affect the magnitude and spatial distribution of drought-induced warming in the continental United States.

We examine this particular aspect of drought in the present paper. Following a brief outline of the DWG experiments in Section 2, we delineate key soil moisture - temperature connections in Section 3. We present in Section 4 the results from the DWG experiments, and in Section 5, we evaluate our findings in the context of available observational data.

2. Overview of US-CLIVAR Working Group Experiments

Again, Schubert et al. (this issue) describe the DWG experiments in detail. In essence, each AGCM simulation is run for 50 years with an idealized set of SST conditions. The imposed SSTs vary monthly but not interannually. The resulting simulation data across the globe are stored for comprehensive analysis; here, we focus on continental precipitation, near-surface air temperature, soil moisture, and net radiation averaged over JJA.

In the present paper, we focus on two experiments in particular:

- (i) PcAn (“Pacific Cold, Atlantic Neutral”). The imposed SSTs are (seasonally varying) climatological SSTs as derived from the 1901-2004 monthly data of Rayner et al. (2002) overlain with a constant (non-seasonally varying) cold anomaly in the Pacific: negative two standard deviations of a rotated empirical orthogonal function (REOF) representing a pan-Pacific ENSO-like pattern that includes a weak Indian Ocean component and no Atlantic component.
- (ii) PwAn (“Pacific Warm, Atlantic Neutral”). In essence, this is the reverse of PcAn: two standard deviations of the pan-Pacific ENSO-like REOF are added to the climatological seasonal cycle.

The two experiments thus represent opposite extremes in Pacific temperature anomalies, with Atlantic anomalies controlled. If Pacific temperatures do have an impact on drought-induced warming, the effect should be clearly seen in the differences between PwAn and PcAn. For context, we sometimes also show or use data from a third experiment, labeled PnAn (for “Pacific Neutral, Atlantic Neutral”), in which the unmodified climatological seasonal cycle of SSTs are imposed.

Five AGCMs performed the DWG experiments: (i) the AGCM of the Global Modeling and Assimilation Office (GMAO) seasonal forecasting effort (Bacmeister et al., 2000), run at $3.75^{\circ} \times 3^{\circ}$ for 50 years (200 years for the PnAn experiment); (ii) the AGCM of the Geophysical Fluid Dynamics Laboratory (GFDL; see Delworth et al., 2006), run at roughly $2^{\circ} \times 2.5^{\circ}$ for 50 years; (iii) the National Center for Atmospheric Research (NCAR) CCM3 AGCM (Kiehl et al., 1998), run at roughly $2.8^{\circ} \times 2.8^{\circ}$ for 50 years; (iv) the NCAR CAM3.5 AGCM, run at roughly $1.4^{\circ} \times 1.4^{\circ}$ for 50 years; and (v) the

National Center for Environmental Prediction (NCEP) GFS AGCM (Campana and Caplan, 2005), run at roughly $1.9^\circ \times 1.9^\circ$ for 36 years.

In the next section, to describe the wetness regime-temperature connection, we focus on data from the GMAO AGCM, because we had full access to this AGCM's complement of auxiliary diagnostic information.

3. Wetness Regime and Temperature

a. Working definition of “dry period temperature”

For the purposes of this paper, we represent the mean JJA (June – August) near-surface air temperature at a given grid cell for a given SST-induced climate by T_{mean} , and we characterize drought-induced warming at the cell through the average JJA temperature (T_{dry}) achieved by that climate during its driest tercile. In more precise terms, T_{dry} for a given climate is defined as the expected value of the JJA temperature conditioned on low (in the lowest tercile) JJA precipitation for that climate, as would occur 1/3 of the time by chance. The PcAn and PwAn simulations produce their own climates and thus their own values of T_{mean} and T_{dry} ; each simulation (and the observational record) is long enough to generate reliable estimates for these quantities.

Note that in much of our analysis, we use deficiencies in time-averaged precipitation rather than in time-averaged soil moisture to define “dryness”, even though soil moisture variations are argued below to have the relevant mechanistic impact on evaporation and thus air temperature. Hydrologically, of course, while lower

precipitation tends to produce drier soil, precipitation and soil moisture are distinct quantities, and thus using precipitation as a proxy for soil moisture incurs some error into our analysis. We nevertheless use precipitation for two reasons: (i) we want to tie our results to observations (section 5), for which soil moisture data are fully inadequate, and (ii) different models produce different “characterizations” of soil moisture (Koster et al., 2009b), implying that a comparison of soil-moisture-related quantities between models is, to a large degree, difficult to interpret – precipitation is a much more straightforward variable to examine. The assumption that precipitation is a workable proxy for soil moisture is supported by K09 and by the AGCM analyses below. It is also supported by maps (not shown) of correlation coefficients generated between JJA soil moisture and JJA precipitation for the five DWG AGCMs. For the GMAO AGCM, the correlation coefficients are 0.7 or higher over most non-desert land areas of the globe; similar levels of correlation are produced by the other AGCMs. While the correlations would presumably be even higher if the JJA soil moistures were correlated against an antecedent precipitation index (API) (i.e., an index that includes information about springtime rainfall), optimizing an API geographically and by model is beyond the scope of this study. For simplicity, this study uses JJA precipitation rates directly.

In subsection (d) below, we relate T_{dry} to three quantities: the mean temperature (T_{mean}), the sensitivity of temperature to precipitation variations within the considered climate, and the variance of precipitation in that climate. This breakdown allows a thorough analysis of the controls on drought-induced warming in a given climate and how these controls change between climates. First, though, to provide context for such a

breakdown, we examine in detail the GMAO AGCM results at a few specific grid cells in the United States.

b. Overall sensitivity of evaporation and temperature to soil moisture: analysis at selected grid cells. The top panels of Figure 2 show, for three grid cells in the United States, the summertime (JJA) relationship between evaporative fraction (EF) and the average degree of saturation in the root zone, as determined from the PnAn, PwAn, and PcAn experiments described in section 2. Each point in each panel corresponds to a single year of one of the three experiments; thus, a total of 300 points are shown (200 from PnAn and 50 from both PwAn and PcAn). The EF curve for the central U.S. grid cell (and at others in this transitional climatic regime) has the general shape suggested by Figure 1; evaporation rates are strongly sensitive to soil moisture variations for degrees of saturation below about 0.5, and they are largely insensitive to soil moisture variations above 0.5. At this grid cell, the attainable soil moistures span a broad range, allowing for an almost complete representation of the curve. The relationships shown for the other two cells (which also represent well their climatic regimes) are also fully consistent with the shape of the curve in Figure 1. However, at these cells, the points span only a subset of the full range. The points for the western U.S. fall only on the dry (water-limited) end of the curve, and those for the eastern U.S. cell fall only on the wet (energy-limited) end.

As argued in section 1 and as demonstrated by K09, a sensitivity of evaporation to soil moisture implies a sensitivity of surface (and thus air) temperature to soil moisture, since more evaporation implies more evaporative cooling. This is clearly illustrated in the middle panels of Figure 2, which show (in analogy to the top panels) the relationship

between average JJA near-surface air temperature and average JJA degree of saturation. For the central United States grid cell, the increase of temperature with decreasing soil moisture is much larger in the drier regime than it is in the wetter regime. (Once again, similar relationships are seen for other grid cells in this area.) The positioning of the transition between regimes is, as expected, strongly consistent with that shown for EF. At the dry western cell, temperatures tend to decrease with increasing soil moisture, consistent with the increases seen for EF. At the wet eastern cell, temperatures are insensitive to soil moisture variations, again consistent with the EF curve.

The bottom panels of Figure 2 show how JJA temperature at the three grid cells varies with JJA precipitation there. Here we introduce the use of JJA precipitation as a proxy for JJA soil moisture (see the discussion above in section 3a). Because average soil moisture typically increases with average precipitation, the behavior indicated in these panels – namely, the increase of temperature with decreasing precipitation in the dry regime and the insensitivity of temperature to precipitation in the wet regime – does not come as a surprise. Again, the central U.S. square includes points in both regimes, and a clear transition is seen between the wetness-sensitive and wetness-insensitive regimes.

The tightness of the cluster of points in both the middle and lower panels, particular for the central U.S. cell, is revealing. JJA temperatures are seen to range from 296K to 314K, and for the most part, these temperature variations are strongly related to soil moisture variations and thus (by proxy) precipitation variations – the higher (lower) temperatures generally do not appear for the wetter (drier) conditions. While such a relationship cannot prove causality, it is strongly consistent with the idea (highlighted in

Figure 1) that soil moisture's impact on evaporation exerts the primary control over near-surface air temperature in this model at the seasonal timescale. Other factors, such as interannual variability in circulation patterns, appear to exert at most a secondary influence.

The Earth system, of course, is highly complex, and thus we must always remain cautious with such statements. To support further the suggested causal mechanisms above, we mention here a valuable supplemental simulation, investigated in K09, that addresses another potential connection between wetness and temperature, one that does not involve the evaporation connection. Conceptually, higher rainfall is associated with greater cloudiness and thus reduced incoming radiation, which could lead to reduced temperatures. In the supplemental simulation, the evaporation connection was artificially disabled – ratios of evaporation to potential evaporation, a function of prognostic temperature, were prescribed to climatological seasonal cycles. K09 found through this simulation that the evaporation connection is dominant by far; the precipitation-radiation connection is, at best, secondary. In essence, the supplemental simulation shows that evaporation variations are necessary in the model to produce the bulk of the simulated JJA temperature variations. Correspondingly, this simulation shows that temperature variations induced by other (non-evaporation-related) mechanisms do not by themselves induce significant evaporation variations. Note that while the evaporation variations presumably act on temperatures mainly through the evaporative cooling mechanism, we cannot rule out, again given the complexity of the Earth system, other possible causal pathways, such as the impact of evaporation variability on cloud variability (e.g., reduced evaporation leads to reduced cloudiness and thus more incoming radiation, heating the

surface). Even if such alternative pathways were important, however, the evaporation variations that are known to affect temperature in the model are still strongly controlled by soil moisture variations, as outlined in Figure 1.

Of course, the impact of evaporation variations on temperature variations is examined here only for JJA. In other seasons, such as March-May, weather systems should have a larger impact on temperature variability [Schubert et al., 2009].

c. Sensitivity of evaporation and temperature to soil moisture in the different SST experiments: analysis at the central U.S. grid cell. The top two panels of Figure 3 are reproductions of the top central panel of Figure 2 (the panel for the central U.S. grid cell), but with the points separated according to SST experiment. Each plot corresponds to a single experiment, with the points from that experiment shown as large red dots and those for the other two experiments (including PnAn) shown as small black dots, for reference. The middle two panels provide the corresponding plots of JJA temperature versus soil moisture at the cell, and the bottom two panels provide the corresponding plots of JJA temperature versus JJA precipitation at the cell.

The plots highlight a very interesting result. The different SST experiments have the effect of “locating” average summer soil moisture or precipitation at the central United States grid cell within different hydroclimatic regimes: the PcAn case generally leads to dry conditions, for which temperature is highly sensitive to moisture variations, whereas the PwAn case leads to much wetter conditions, with correspondingly reduced sensitivity.

d. *Drought-induced warming: Separating the impacts of changes in mean and changes in sensitivity.* The two panels in Figure 4 are annotated versions of the bottom two panels of Figure 3, with points shown only for the climate in question. In each panel, the blue circle on the right locates the mean JJA precipitation and temperature for the climate (P_{mean} and T_{mean}), and the blue circle on the left locates the average JJA precipitation and temperature obtained during the climate's driest tercile (P_{dry} and T_{dry}). Linear regression is used to fit a line (with slope "dT/dP") through all the black points, which represent data for individual years. (Despite the underlying nonlinearity in the relationship, we use all the points rather than just those within the "dry region" of the plot to produce a more robust estimate of the slope. This could lead to error, but as shown below, such error is small.) In the figure, $\Delta_{\text{dry}}P$ refers to the difference between P_{dry} and P_{mean} – i.e., the average degree to which the driest tercile of years is indeed drier than the climatic mean.

Given these definitions, an equation for estimating T_{dry} (which we will use to characterize drought-induced warming) from T_{mean} , dT/dP , and $\Delta_{\text{dry}}P$ becomes obvious:

$$T_{\text{dry-est}} = T_{\text{mean}} + \Delta_{\text{dry}}P (dT/dP) \quad (1)$$

Note from the figure that for PcAn, T_{mean} is warmer and the sensitivity of T to precipitation variations is higher than for PwAn. As a result of both factors, $T_{\text{dry-est}}$ is warmer for PcAn.

Following immediately from this equation is one that relates that *change* in T_{dry} between the PcAn and PwAn climates (denoted as $\Delta_{\text{PcAn-PwAn}} []$) to climatic changes in T_{mean} , dT/dP , and $\Delta_{\text{dry}}P$:

$$\Delta_{\text{PcAn-PwAn}} [T_{\text{dry-est}}] = \Delta_{\text{PcAn-PwAn}} [T_{\text{mean}}] + \Delta_{\text{PcAn-PwAn}} [\Delta_{\text{dry}}P (dT/dP)] \quad (2)$$

Written in this way, the ability of a shift in climate (as induced by a shift in SSTs) to affect temperature during dry periods is clearly related to both the shift in the mean climate (the first addend on the RHS of (2)) and a climatic shift in the sensitivity of temperature to precipitation (the second addend). The two effects are compared quantitatively in the analysis below.

4. AGCM Results

In one sense, the central U.S. grid cell examined in Figure 3 is not strictly representative of the continental United States; it was chosen precisely because the soil moistures produced by the different experiments were distinctly different, allowing for the clearest illustration of potential SST impacts in terms of both changes in mean temperature and changes in temperature sensitivity. Nevertheless, for the GMAO system, all United States grid cells show the same tight clustering around single underlying relationships of the type shown in Figure 2, and in terms of SST-related differences, most in the central United States behave much like the one examined in Figure 3. Furthermore, scatter plots (not shown) of JJA temperature versus JJA precipitation for the other AGCMs show similar structure to that shown in the bottom panels of Figure 2, implying that the same underlying mechanisms are at work in these models as well. Now, using (2), we examine, on a continental scale, the extent to which different SST regimes affect T_{dry} through changes in T_{mean} , dT/dP , and $\Delta_{\text{dry}}P$.

a. *Test of linearization: continental maps.* We first demonstrate with Figure 5 that the linearization in (2) is indeed valid. The top five rows show, for each of the participating models, continental comparisons between $\Delta_{\text{PcAn-PwAn}} [T_{\text{dry-est}}]$ (left column) and the actual value of $\Delta_{\text{PcAn-PwAn}} [T_{\text{dry}}]$ computed from the model diagnostics (right column). We plot differences between the climates rather than the values for the two climates separately to maintain parsimony in figures and because we are mostly interested in how the two climates differ from each other – PcAn and PwAn represent extremes in SST forcing, and it is in the difference between these extremes that we expect to find the strongest signals. Notice the addition in the colorbar of an extra shading contour at 0.5 degrees.

The AGCMs show many differences in $\Delta_{\text{PcAn-PwAn}} [T_{\text{dry}}]$, with particularly strong values in the Great Plains for GMAO, weaker values for CCM3, CAM3, and GFDL, and an almost complete lack of signal for GFS, despite the fact that it does show lower precipitation for PcAn than for PwAn. [The anomalous behavior of GFS relative to the other models is discussed further by Schubert et al. (2009).] The agreement, however, between $\Delta_{\text{PcAn-PwAn}} [T_{\text{dry-est}}]$ and $\Delta_{\text{PcAn-PwAn}} [T_{\text{dry}}]$ for any given AGCM is remarkably strong. This supports the use of (2) to separate climatic changes in drought-induced warming ($\Delta_{\text{PcAn-PwAn}} [T_{\text{dry}}]$) into contributions from changes in T_{mean} and changes in temperature sensitivity, and in particular, to explain why $\Delta_{\text{PcAn-PwAn}} [T_{\text{dry}}]$ differs so much geographically and between the models.

b. *Relative contributions of the T_{mean} and $\Delta_{\text{dry}}P(dP/dT)$ terms.* Given this strong agreement, we are justified in presenting in Figure 6 the continental maps of the two

terms contributing to $T_{\text{dry-est}}$, namely, T_{mean} and $(\Delta_{\text{dry}}P)(dT/dP)$. Again, what we in fact show are the climatic differences (PcAn minus PwAn) in the “mean” term ($\Delta_{\text{PcAn-PwAn}} [T_{\text{mean}}]$; right panels) and the temperature sensitivity term ($\Delta_{\text{PcAn-PwAn}} [\Delta_{\text{dry}}P(dT/dP)]$, left panels). The same colorbar is used for each column, allowing a direct comparison of the magnitudes of the two terms.

The figure clearly shows, for the first four AGCMs, that the differences in T_{dry} between the two climates stem mostly from differences in T_{mean} . In other words, in the central United States, PcAn SSTs generally produce drier and thus warmer conditions than PwAn SSTs, and this overall relative warming is directly reflected in the driest years as well. (Again, the fifth AGCM, GFS, shows almost no temperature signal at all, though it does show drier conditions for the PcAn case.) Even so, for at least three of the AGCMS (GMAO, CCM3, and CAM3), there appears to be a significant additional contribution to the climatic change in T_{dry} from the term involving temperature sensitivity, $(\Delta_{\text{dry}}P)(dT/dP)$. In direct agreement with Figure 3, the change in SST-induced climate appears in some places – particularly in parts of the central and eastern United States – to change the temperature regime from being (relatively) insensitive to interannual moisture variations (for PwAn) to being sensitive to them (for PcAn).

Indeed, the location of the central U.S. grid cell examined in Figures 2 through 4 is located in the top panels of Figure 6. As indicated in Figure 4, the high value for $\Delta_{\text{PcAn-PwAn}} [(\Delta_{\text{dry}}P)(dT/dP)]$ at this location stems almost exclusively from the higher slope (dT/dP) seen for the PcAn climate, since the PcAn and PwAn values of $\Delta_{\text{dry}}P$ appear similar. For GFDL, on the other hand, the $(\Delta_{\text{dry}}P)(dT/dP)$ term appears to *reduce* slightly the impact of the imposed SST states on T_{dry} , and since the slope (dT/dP) is not generally

reduced under the drier conditions induced by PcAn for GFDL, we hypothesize that the variance of precipitation for PcAn must have been reduced instead. To examine these behaviors more thoroughly, we call upon the following mathematical identity:

$$\Delta_{\text{PcAn-PwAn}} [(\Delta_{\text{dry}}P)(dT/dP)] = \overline{\Delta_{\text{dry}}P} \Delta_{\text{PcAn-PwAn}} [dT/dP] + \overline{dT/dP} \Delta_{\text{PcAn-PwAn}} [(\Delta_{\text{dry}}P)], \quad (3)$$

where the overbar represents the average between the values for the PcAn and PwAn climates. The first and second terms on the right describe, respectively, the separate impacts of climatic changes in temperature sensitivity (dT/dP) and precipitation variance ($\Delta_{\text{dry}}P$) on the climatic change in $(\Delta_{\text{dry}}P)(dT/dP)$, using equivalent units.

We present these two separate impacts separately for each AGCM in Figure 7. In many areas (except for the center of the U.S. in GMAO, where the opposite occurs), changes in precipitation variance between the PcAn and PwAn climates reduce the impact of the change in climates on T_{dry} . Simply put, in many regions precipitation does not decrease as much during dry periods for PcAn as it does for PwAn, and, as suggested in Figure 4 and equation (2), this would have a mitigating effect on drought-induced warming for PcAn. This effect, however, is more than counteracted for in GMAO, CAM3, and CCM3 by the associated increase in the sensitivity of temperature to rainfall (the slope term: left panels of Figure 7); the net result, as shown in Figure 6, is a generally positive impact of the $(\Delta_{\text{dry}}P)(dT/dP)$ term on $\Delta_{\text{PcAn-PwAn}} [\Delta T_{\text{dry}}]$.

5. Observations

We now attempt an “observational” version of the analysis presented above. First, we composite observational years according to whether certain aspects of their JJA SST distributions are similar to those used for the PcAn and PwAn experiments. We then treat each composited set of years as an analogue to the corresponding idealized simulation.

a. *Compositing rules.* Years are composited based on the Nino3 index, defined as the average temperature anomaly in the tropical Pacific between 5°N and 5°S and between 150°W and 90°W. (The Nino3 data were provided by the NOAA-ESRL Physical Sciences Division, Boulder, Colorado, via their web site: <http://www.esrl.noaa.gov/psd/>.) Although the strength of the Nino3 signal is relatively weak for JJA (e.g., An and Choi, 2009), we use JJA averages of the Nino3 index in the compositing, given this paper’s focus on boreal summer.

We compute the mean (μ) and standard deviation (σ) of JJA Nino3 and then composite the measurement years as follows:

$$\begin{aligned}
 &\text{neutral Pacific years (PnAn analogue): } \mu - \alpha\sigma < \text{Nino3} < \mu + \alpha\sigma \\
 &\text{cold pacific years (PcAn analogue): } \text{Nino3} < \mu - \alpha\sigma \\
 &\text{warm Pacific years (PwAn analogue): } \text{Nino3} > \mu + \alpha\sigma
 \end{aligned}
 \tag{4}$$

Here, α is chosen as 0.43, which for a normal distribution divides the distribution into thirds. The PcAn and PwAn composited observational analogues consist of 35 and 34 years of data, respectively, out of a total of 107 years.

JJA temperatures and precipitations over the United States are composited over these years to compute mean near-surface air temperatures and precipitations for the different SST regimes and to compute temperature anomalies for the driest tercile within an SST regime. In other words, we compute from these data observational proxies for $\Delta_{\text{PcAn-PwAn}} [T_{\text{dry}}]$, $\Delta_{\text{PcAn-PwAn}} [T_{\text{dry-est}}]$, $\Delta_{\text{PcAn-PwAn}} [T_{\text{mean}}]$, and $\Delta_{\text{PcAn-PwAn}} [\Delta_{\text{dry}}P (dT/dP)]$. The temperature and precipitation data are derived from GHCN gridded observations (for details, see <http://www.ncdc.noaa.gov/oa/climate/research/ghcn/ghcngrid.html>), which cover the period 1900-present at a resolution of $5^{\circ} \times 5^{\circ}$.

b. *Limitations to observational study.* Before the observational analysis proceeds, four important limitations of the analysis must be emphasized. First, the observed SSTs within a given year of a composite will never match the idealized distribution used in the PcAn or PwAn experiments. For the PcAn case, for example, the AGCM prescribes a specific EOF pattern in the Pacific and assigns (for the most part) neutral conditions everywhere else. In contrast, in our observational analysis, a year marked as having “cold Pacific” conditions may have warm tropical Pacific conditions outside the Nino3 region, and it may certainly have non-neutral (perhaps warm, perhaps cold) conditions in the tropical Atlantic and in all of the subtropical and midlatitude oceans. The comparisons between the AGCM results and the observational data will thus never be exact.

The second limitation involves the magnitudes of the Nino3 SST conditions considered. The PcAn and PwAn experiments effectively imposed SST EOF patterns amounting to 2 standard deviations from the mean. In order to obtain sufficient years for

our statistics, the observational analysis is forced to examine SST anomalies of much smaller size. The resulting signals over the continents are thus expected to be weaker, perhaps substantially so. The third limitation again has to do with the sample size. Even with the reduced threshold imposed for the Nino3 anomaly, the observations provide only about 35 years for both PcAn and PwAn, a smaller sample size than obtained with most of the AGCM experiments.

Finally, and perhaps most importantly, we must accept the fact that the observations are likely to contain significant errors. SST errors, for example, are much larger early on (Smith and Reynolds, 2004). Continental precipitation and temperature data in the early years are based on spotty measurements and are thus subject to substantial representativeness error. We can expect substantial noise in any derived relationships from these errors alone.

c. Results. With these caveats in mind, we present the observational results in the bottom panels of Figures 5-7. Because all signals are necessarily smaller due to the smaller SST variations considered (see the second limitation noted above), all PcAn – PwAn differences are multiplied by four before plotting.

The first result, at the bottom of Figure 5, is that the linearization embodied in (2) works well for the observations, though not as well as it does for the AGCMs. The reduced performance is undoubtedly due to the relatively higher noise in the observational data, which leads to underestimates of the dP/dT slope. The agreement is still adequate enough, however, to proceed with the observational analysis.

The bottom panels of Figure 6 show that the relative impacts of the mean and sensitivity terms on $\Delta_{\text{PcAn-PwAn}} [T_{\text{dry}}]$ are generally similar to those shown for GMAO, CCM3, and CAM3. The observations, however, show a larger areal impact of the sensitivity term, one that extends across a broader north-south swath of the central United States. The sensitivity term in the central U.S. is also stronger for the observations than for the AGCMs in terms of its fractional contribution to T_{dry} , relative to the T_{mean} term.

The bottom panels of Figure 7 shows that the larger impact of the sensitivity term mostly reflects a large change, between the PcAn and PwAn climates, in the dT/dP slope. The change in $\Delta_{\text{dry}}P$ between the two climates is quite small. The negative slope differences seen in the far west and far east for the observations are presumably a result of noise in the data.

d. *Interpretation of observed T_{dry} relative to multi-decadal climatology.* In the above analysis, T_{dry} for a given climate is defined according to the range of moisture conditions for that particular climate. How, though, does T_{dry} compare to the long-term mean JJA value, $T_{\text{mean,all-SST}}$, for a region exposed to the full range of interannual variations in SST? A comparison of T_{dry} to $T_{\text{mean,all-SST}}$ would be especially illuminating, since it would address the following question: compared to the long-term average JJA temperature observed for a region, what is the expected value of the JJA temperature anomaly in a given year conditioned on two things: (i) SST distribution, and (ii) JJA precipitation falling within the driest tercile for that SST distribution (i.e., that would occur by chance, one-third of the time)?

For the observational proxies to the PcAn and PwAn climates considered, Figure 8 shows the expected values of T_{mean} minus $T_{\text{mean,all-SST}}$ (top panels) and T_{dry} minus $T_{\text{mean,all-SST}}$ (bottom panels). Considering the top panels first, we see that in nature, a cold (warm) Pacific tends to lead to higher (lower) mean temperatures in the central United States, relative to long-term climatology. (Again, this reflects changes in precipitation, not shown, relative to long-term means.) The bottom panels in turn show that for both cold and warm conditions in the Pacific, nature produces warm anomalies in the central U.S. during the driest third of years for those conditions. The warm anomalies are, as expected, much higher for cold Pacific conditions, exceeding a degree in some places.

Note that the difference between the bottom two panels is greater than the difference between the top two panels, implying that SST conditions have a larger impact on T_{dry} anomalies than on T_{mean} anomalies. By definition, the two differences correspond exactly to the bottom right panel of Figure 5 and the bottom right panel of Figure 6, respectively. As illustrated in the analyses above, SST impacts on T_{dry} are larger because the SST-induced shifts in hydrological regime have an impact on the *sensitivity* of temperature to moisture variations as well as on the mean temperature itself.

A fifth caveat, however, should be mentioned here. The observational results are somewhat sensitive to the choice of α in the compositing rules listed above. Recall that α in (4) was set to 0.43 to divide the observed years into thirds. The strong relative contribution of the temperature sensitivity term to T_{dry} in the bottom panels of Figure 6 is maintained for lower values of α , but it is reduced somewhat for higher values of α (e.g., 0.6). Of course, with higher values of α , fewer years contribute to the PcAn and PwAn composites, contributing to sampling error.

Finally, for a more concrete historical perspective, the plots in Figure 9 show the time history of the Nino3 index and an estimate of its impact on soil moisture and temperature in the U.S. Great Plains (105W – 95W, 30N – 49N; see the region outlined in the lower left panel of Figure 8). Figure 9a shows the Nino3 index for JJA, as averaged over 6-year periods starting in 1920. Figures 9b and 9c show soil moisture and surface temperature in the Great Plains for these 6-year periods as generated by a land surface model (the catchment model of Koster et al. [2000]) driven for 80 years with observations-based meteorological forcing across the continental United States (Wang et al., in press). The period with the lowest JJA Nino3 index (1932-37) shows both the lowest average soil moisture and, correspondingly, the highest average surface temperature, whereas the period with the highest Nino3 index (1992-97) shows both the highest average soil moisture and the lowest average surface temperature. Furthermore, the slope of the EF-soil moisture relationship (not shown) is indeed relatively high for 1932-37 and relatively low for 1992-1997. While the results for the extreme Nino3 periods are thus in agreement with the discussions above, we also see that Nino3 is not the only control over soil moisture and temperature behavior in the Great Plains. The period 1944-1949, for example, shows a low value for the index but features a relatively high soil moisture content.

6. Summary

The USCLIVAR DWG numerical experiments provide a unique environment for addressing an important climatic question, namely, to what extent is drought-induced warming (i.e., the tendency for drier-than-average summertime conditions to induce

warmer-than-average conditions on a seasonal timescale) influenced by SST distribution? The different AGCMs generally show that the distinction between cold and warm Pacific conditions leads to a difference in drought-induced warming in the central United States, with the warming relatively enhanced for cold Pacific conditions for two separate reasons, both related to the fact that the cold Pacific induces a drier hydrological regime: (i) the overall change in mean JJA temperatures, and (ii) the change in within-climate temperature sensitivity to interannual moisture variations. The location of sensitivity in central North America is not surprising given the region's hydroclimatic character, known from past studies (e.g., Koster et al., 2003, 2004) to lie at the critical transition between very wet and very dry conditions.

These results are supported by a joint analysis of gridded observed JJA precipitation and air temperature. Figure 8 shows in particular that during relatively dry conditions (as occur by chance one-third of the time) for the cold Pacific case, the expected value of the temperature anomaly in the central United States can be higher than 1°C (a considerable anomaly given that it refers to a full seasonal mean), whereas the corresponding anomaly for warm Pacific conditions is much less. Overall, the results are sensible when considered in the context of both the idealized “EF curve” illustrated in Figure 1 and the overall changes in dryness induced by the different SST distributions. In this sense, the results showcase the potentially complex interactions between ocean-land teleconnections and land-based hydroclimatic controls on evaporation.

Acknowledgments. This work was carried out as part of a U.S. CLIVAR drought working group activity supported by NASA, NOAA, and NSF to coordinate and compare climate model simulations forced with a common set of idealized SST patterns. The authors would like to thank NASA's Global Modeling and Assimilation Office (GMAO) for making the NSIPP1 runs available, the Lamont-Doherty Earth Observatory of Columbia University for making their CCM3 runs available, NOAA's Environmental Modeling Center (EMC) and Climate Prediction Center (CPC) for making the GFS runs available, NOAA's Geophysical Fluid Dynamics Laboratory (GFDL) for making the AM2.1 runs available, the National Center for Atmospheric Research (NCAR) for making the CAM3.5 runs available, and the Center for Ocean Land Atmosphere (COLA) and the University of Miami's Rosenstiel School of Marine and Atmospheric Science for making the CCSM3.0 coupled model runs available.

References

- An, S-I, and J. Choi, 2009: Seasonal locking of the ENSO asymmetry and its influence on the season cycle of the tropical eastern Pacific sea surface temperature. *J. Geophys. Res.*, in press.
- Bacmeister J., P. J. Pegion, S. D. Schubert, and M. J. Suarez, 2000: An atlas of seasonal means simulated by the NSIPP 1 atmospheric GCM. Vol. 17. NASA Tech. Memo. 104606, Goddard Space Flight Center, Greenbelt, MD, 194 pp.
- Budyko, M. I., 1974: *Climate and Life*. Academic Press, New York, 508 pp.
- Campana, K. and P. Caplan, Editors, 2005: Technical Procedure Bulletin for T382 Global Forecast System (http://www.emc.ncep.noaa.gov/gc_wmb/Documentation/TPBoct05/T382.TPB.FI.NAL.htm).
- Chang, F.-C., and J. M. Wallace, 1987: Meteorological conditions during heat waves and droughts in the United States Great Plains. *Mon. Wea. Rev.*, **115**, 1253-1269.
- Delworth et al., 2006: GFDL's CM2 global coupled climate models - Part 1: Formulation and simulation characteristics, *J. Climate*, **19**, 643-674.
- Durre, I., J. M. Wallace, and D. P. Lettenmaier, 2000: Dependence of extreme daily maximum temperatures on antecedent soil moisture in the contiguous United States during summer. *J. Climate*, **13**, 2641-2651.
- Eagleson, P. S., 1978: Climate, soil and vegetation, 4, The expected value of annual evapotranspiration. *Water Resour. Res.*, **14**, 731-739.

- Huang, J., H. M. van den Dool, and K. Georgakakos, 1996: Analysis of model-calculated soil moisture over the United States (1931-1993) and applications to long-range temperature forecasts. *J. Climate*, **9**, 1350-1362.
- Karl, T. R., 1986: The relationship of soil moisture parameterizations to subsequent seasonal and monthly mean temperature in the United States. *Mon. Wea. Rev.*, **114**, 675-686.
- Kiehl, J.T., J.J. Hack, G. Bonan, B.A. Boville, D. Williamson and P. Rasch, 1998. The National Center for Atmospheric Research Community Climate Model: CCM3. *J. Climate*, **11**, 1131-1149.
- Koster, R. D., M. J. Suarez, A. Ducharne, M. Stieglitz, and P. Kumar, 2000: A catchment-based approach to modeling land surface processes in a general circulation model, I, Model structure. *J. Geophys. Res.*, **105**, 24809-24822.
- Koster, R. D., R. W. Higgins, H. Van den Dool, and M. J. Suarez, 2003: Observational evidence that soil moisture variations affect precipitation. **Geophysical Research Letters**, *30*(5), 1241, doi:10.1029/2002GL016571.
- Koster, R. D., P. A. Dirmeyer, Z. Guo, and 22 others, 2004: Regions of strong coupling between soil moisture and precipitation. **Science**, *305*, 1138-1140.
- Koster, R. D., S. Schubert, and M. J. Suarez, 2009a: Analyzing the concurrence of meteorological droughts and warm periods, with implications for the determination of evaporative regime. **J. Climate**, in press.
- Koster, R. D., Z. Guo, R. Yang, P. A. Dirmeyer, K. Mitchell, and M. J. Puma, 2009b: On the nature of soil moisture in land surface models. *J. Climate*, in press.

- Manabe, S., 1969: Climate and the ocean circulation, I, The atmospheric circulation and the hydrology of the Earth's surface. *Mon. Wea. Rev.*, **97**, 739-774.
- Namias, J., 1960: Factors in the initiation, perpetuation and termination of drought. Extract of Publ. 51, International Association of Hydrological Sciences (IAHS) Commission of Surface Waters, 81-94. [Available from IAHS Press, Institute of Hydrology, Wallingford, Oxfordshire, OX10 8BB, United Kingdom.]
- Rayner, N.A., D.E. Parker, E.B. Horton, C.K. Folland, L.V. Alexander, D.P. Rowell, E.C. Kent, A. Kaplan, 2002: Global analyses of SST, sea ice and night marine air temperature since the late nineteenth century. *J. Geophys. Res.* 108, 4407, doi:10.1029/2002JD002670 (2003).
- Schubert, S. D., and Co-Authors, 2009: A USCLIVAR project to assess and compare the responses of global climate models to drought-related SST forcing patterns, Overview and results. **J. Climate**, in review.
- Shinoda, M., and Y. Yamaguchi, 2003: Influence of soil moisture anomaly on temperature in the Sahel: A comparison between wet and dry decades. *J. Hydromet.*, **4**, 437-447.
- Smith, T. M., and R. W. Reynolds, 2004: Improved extended reconstruction of SST (1854-1997). *J. Climate*, **17**, 2466-2477.
- Wang, A., T. J. Bohn, S. P. Mahanama, R. D. Koster, and D. P. Lettenmaier, 2009: Multi-model ensemble reconstruction of drought over the continental United States. **J. Climate**, in press.

Figure Captions

Figure 1. Idealized picture of the so-called “EF curve”, showing a strong sensitivity of evaporative fraction EF (the ratio of evaporation to net radiation) to soil moisture in the drier regime and a minimal sensitivity in the wetter regime.

Figure 2. Relationships diagnosed from GMAO AGCM diagnostics. Top panels: JJA evaporative fraction (EF) versus JJA average soil moisture w (degree of saturation). Middle panels: JJA temperature (K) versus JJA soil moisture (degree of saturation). Bottom panels: JJA temperature (K) versus JJA precipitation (mm/day). The three grid cells examined (one for each column) are representative of three climatic regimes (dry, transitional, and wet) in the U.S. See the top row of Figure 6 for the location of the central U.S. grid cell, which is examined further in Figures 3 and 4.

Figure 3. Top panels: same as the top central panel of Figure 2, but with the points separated according to the imposed SST distributions. The red dots are those from the labeled SST experiment. Middle panels: same (again for the central U.S. grid cell), but for the relationship between JJA temperature (K) and JJA soil moisture (degree of saturation). Bottom panels: same, but for the relationship between JJA temperature (K) and JJA precipitation (mm/day).

Figure 4. Illustration of quantities used in (1). Top: JJA temperature vs. JJA precipitation for the PcAn climate at the grid cell considered in Figures 2 and 3. Each dot represents a different year. Overlain on the plot is the fitted regression line (in red), the point representing the mean JJA temperature and precipitation for the PcAn climate (rightmost blue circle), that representing the average JJA temperature and precipitation in the driest precipitation tercile for that climate (leftmost blue circle), and the difference between the two precipitation averages. Bottom: Same, but for the PwAn climate.

Figure 5. Test of linearized approximation in equation (2). Left panels: $\Delta_{\text{PcAn-PwAn}} [T_{\text{dry-est}}]$, as calculated with (2), for the five AGCMs and for the observational data. Right panels: $\Delta_{\text{PcAn-PwAn}} [T_{\text{dry}}]$, as computed directly from the temperatures themselves. Units are $^{\circ}\text{C}$. Values for the observational data are multiplied by four prior to plotting, to reflect (qualitatively) the weaker SST signal examined.

Figure 6. Relative magnitudes of the $\Delta_{\text{PcAn-PwAn}} [\Delta_{\text{dry}}P (dT/dP)]$ and $\Delta_{\text{PcAn-PwAn}} [T_{\text{mean}}]$ terms contributing to the difference $T_{\text{dry}}(\text{PcAn}) - T_{\text{dry}}(\text{PwAn})$, as outlined in equation (2). Units are $^{\circ}\text{C}$. The black circle in the top row panels locates the grid cell examined in Figures 3 and 4. Values for the observational data are multiplied by four prior to plotting, to reflect (qualitatively) the weaker SST signal examined.

Figure 7. Relative contributions of the “temperature sensitivity” (dT/dP) and “precipitation variance” ($\Delta_{dry}P$) terms to the $\Delta_{dry}P$ (dT/dP) differences shown in Figure 6, as outlined in equation (3). Units are $^{\circ}C$. Values for the observational data are multiplied by four prior to plotting, to reflect (qualitatively) the weaker SST signal examined.

Figure 8. Top left: Values of observed T_{mean} (in $^{\circ}C$) for proxy PcAn conditions minus the long term average JJA temperature for all SST conditions. Top right: Same, but for proxy PwAn conditions. Bottom left: Values of observed T_{dry} (in $^{\circ}C$) for proxy PcAn conditions minus the long term average JJA temperature for all SST conditions. (The outlined region is examined further in Figure 9.) Bottom right: Same, but for PwAn conditions.

Figure 9. a. Average of Nino3 index (for JJA) over six year periods spanning 1920 to 2003. b. Corresponding average soil moisture (volumetric) in the U.S. Great Plains, as simulated in an extended offline simulation with a land surface model driven with observations-based forcing. c. Corresponding surface temperature in the U.S. Great Plains, as established through the same offline simulation.

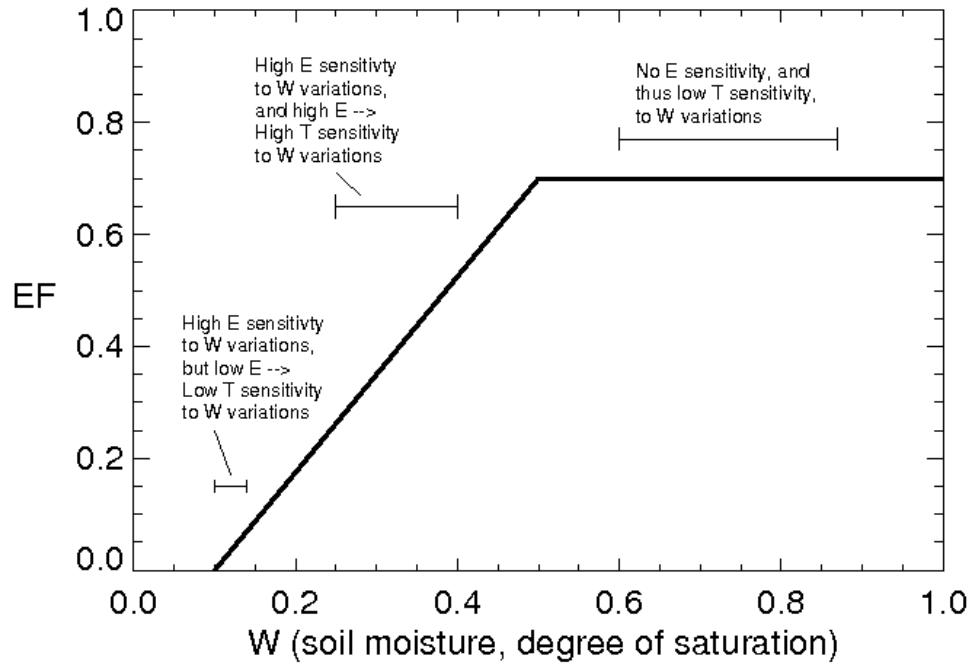


Figure 1. Idealized picture of the so-called “EF curve”, showing a strong sensitivity of evaporative fraction EF (the ratio of evaporation to net radiation) to soil moisture in the drier regime and a minimal sensitivity in the wetter regime.

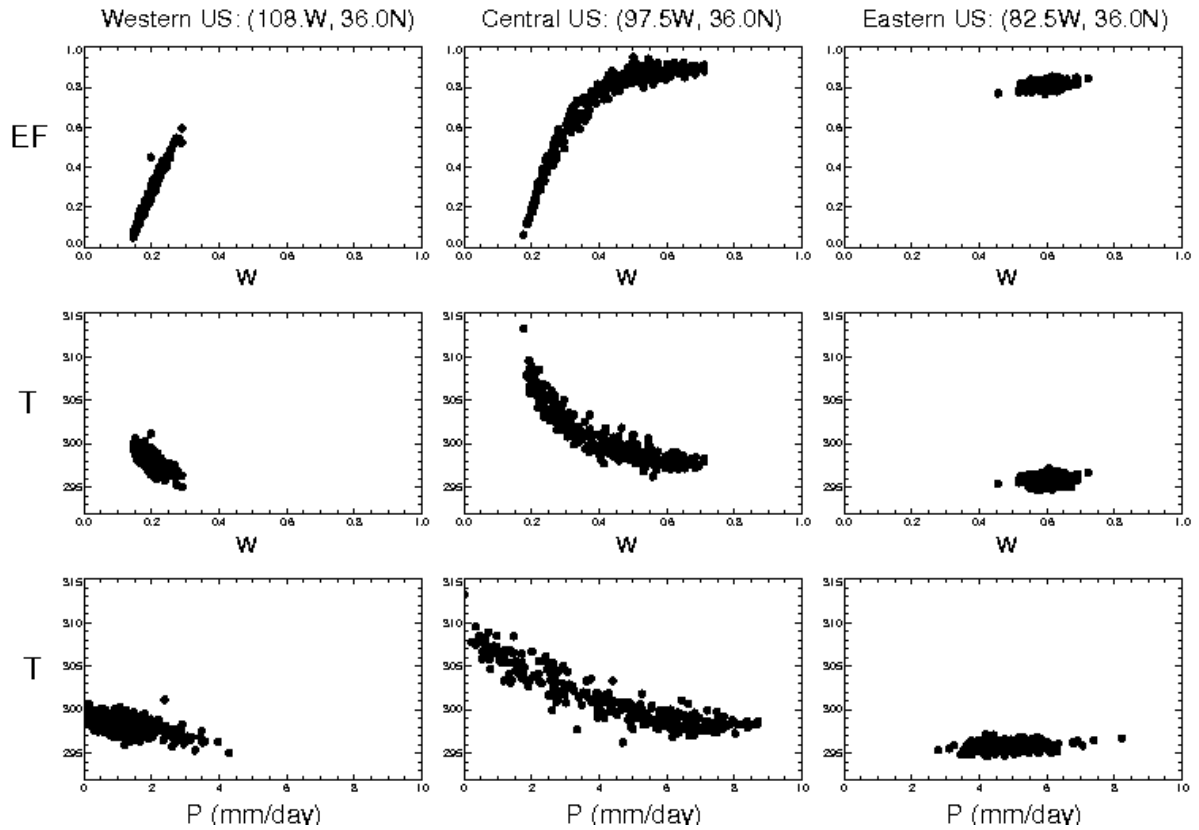


Figure 2. Relationships diagnosed from GMAO AGCM diagnostics. Top panels: JJA evaporative fraction (EF) versus JJA average soil moisture w (degree of saturation). Middle panels: JJA temperature (K) versus JJA soil moisture (degree of saturation). Bottom panels: JJA temperature (K) versus JJA precipitation (mm/day). The three grid cells examined (one for each column) are representative of three climatic regimes (dry, transitional, and wet) in the U.S. See the top row of Figure 6 for the location of the central U.S. grid cell, which is examined further in Figures 3 and 4.

Central US Grid Cell

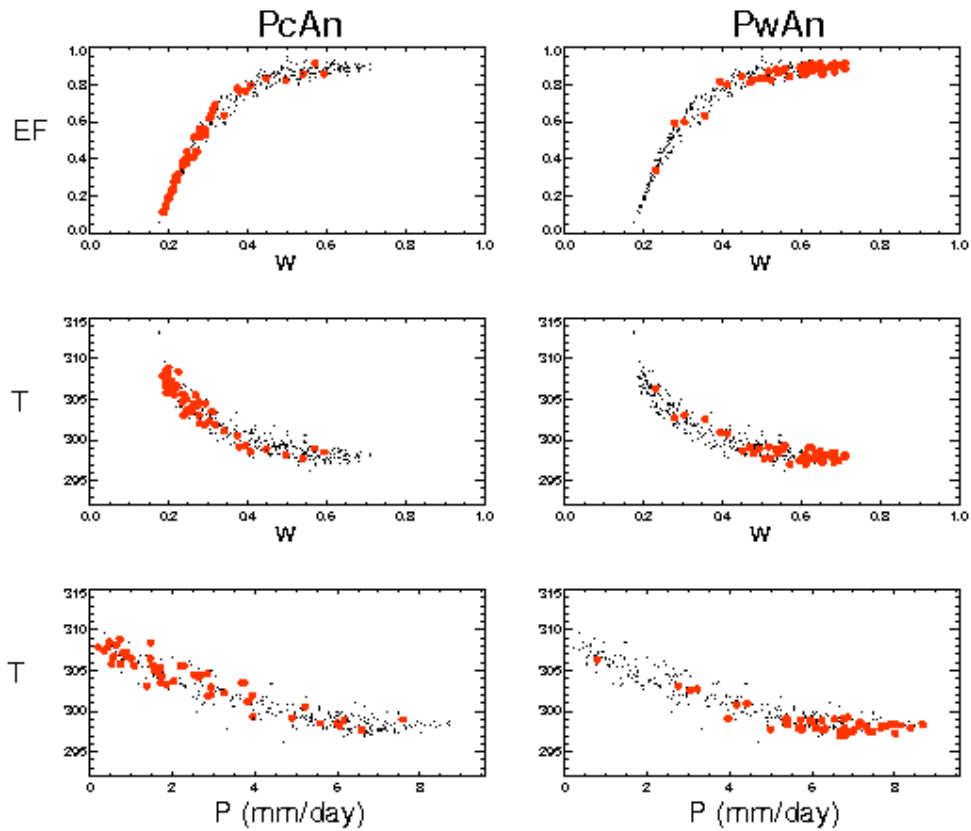


Figure 3. Top panels: same as the top central panel of Figure 2, but with the points separated according to the imposed SST distributions. The red dots are those from the labeled SST experiment. Middle panels: same (again for the central U.S. grid cell), but for the relationship between JJA temperature (K) and JJA soil moisture (degree of saturation). Bottom panels: same, but for the relationship between JJA temperature (K) and JJA precipitation (mm/day).

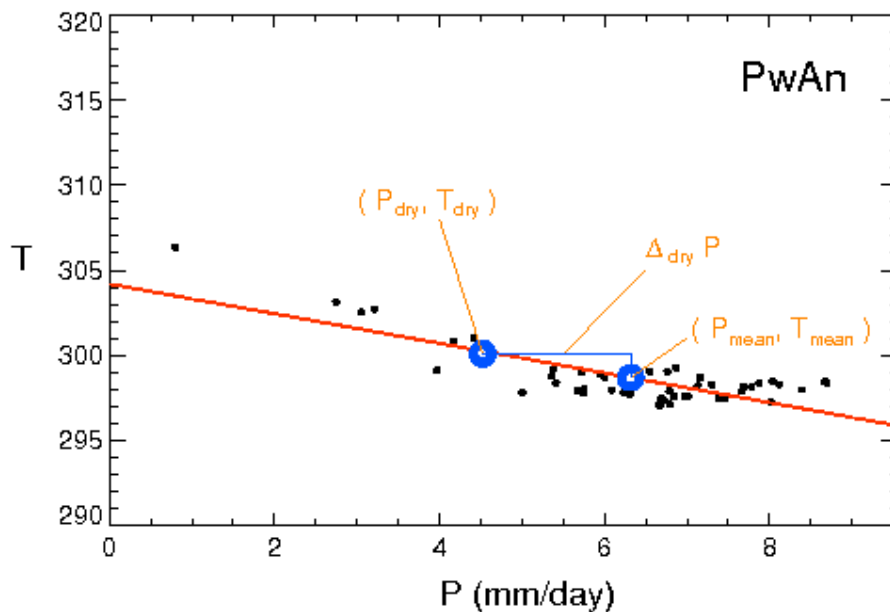
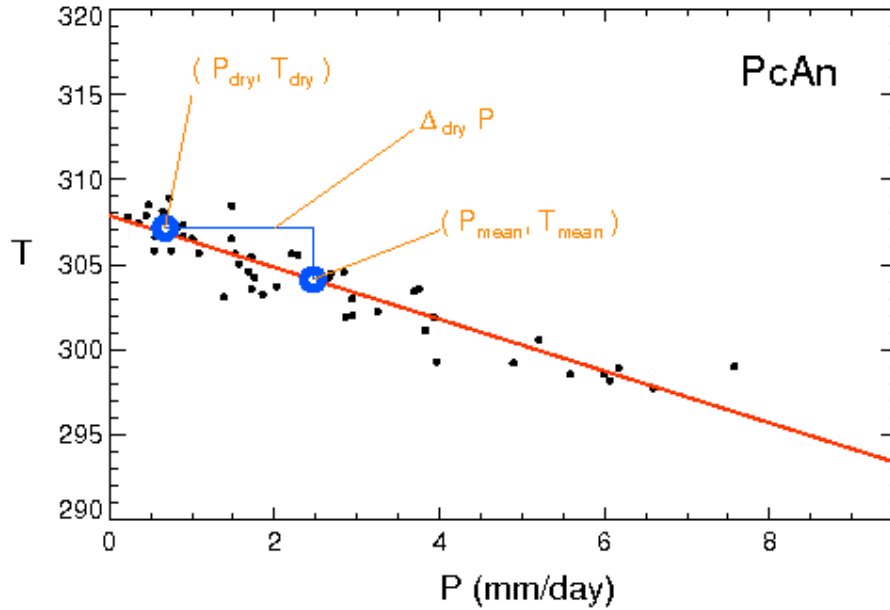


Figure 4. Illustration of quantities used in (1). Top: JJA temperature (K) vs. JJA precipitation for the PcAn climate at the grid cell considered in Figures 2 and 3. Each dot represents a different year. Overlain on the plot is the fitted regression line (in red), the point representing the mean JJA temperature and precipitation for the PcAn climate (rightmost blue circle), that representing the average JJA temperature and precipitation in the driest precipitation tercile for that climate (leftmost blue circle), and the difference between the two precipitation averages. Bottom: Same, but for the PwAn climate.

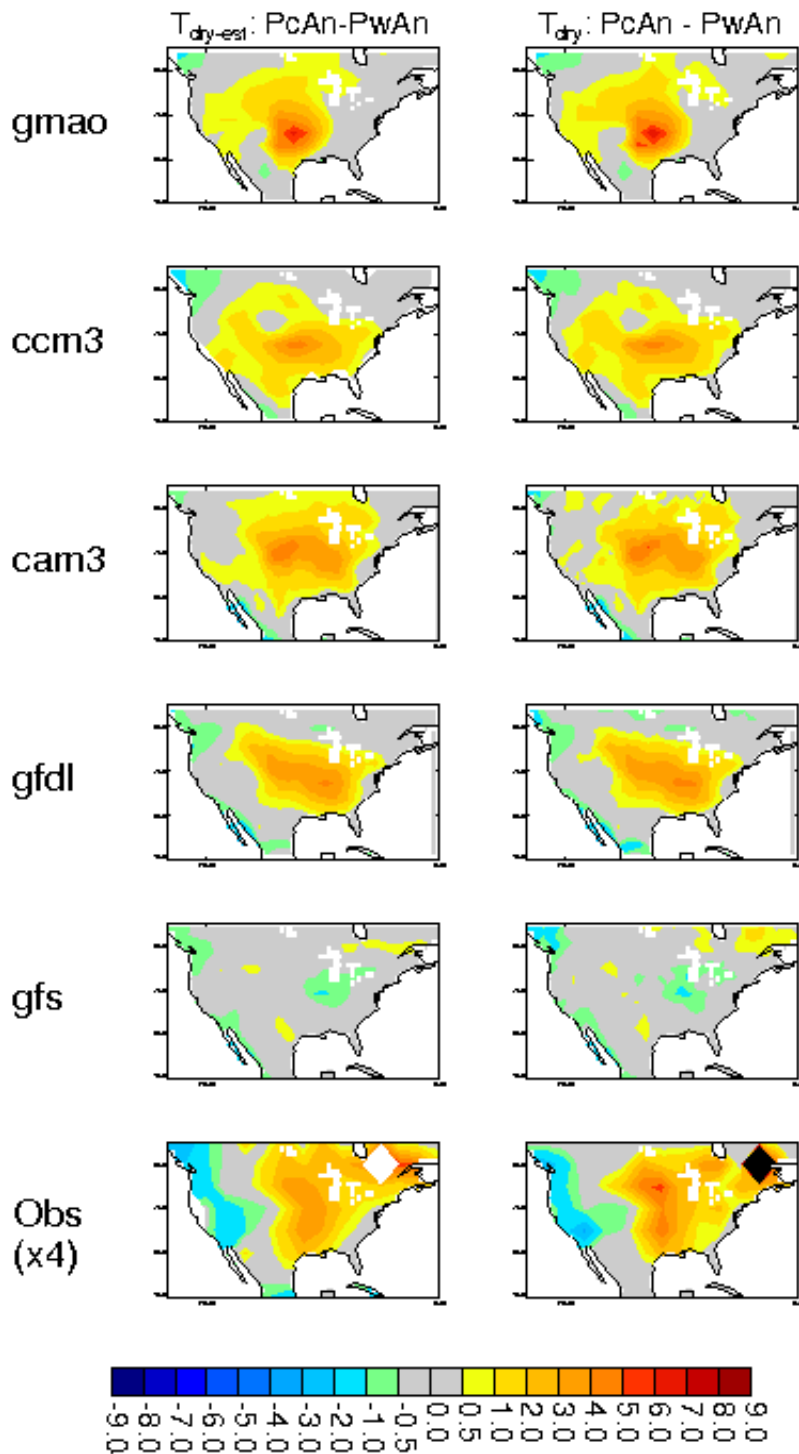


Figure 5. Test of linearized approximation in equation (2). Left panels: $\Delta_{\text{PcAn-PwAn}} [T_{\text{dry-est}}]$, as calculated with (2), for the five AGCMs and for the observational data. Right panels: $\Delta_{\text{PcAn-PwAn}} [T_{\text{dry}}]$, as computed directly from the temperatures themselves. Units are $^{\circ}\text{K}$. Values for the observational data are multiplied by four prior to plotting, to reflect (qualitatively) the weaker SST signal examined.

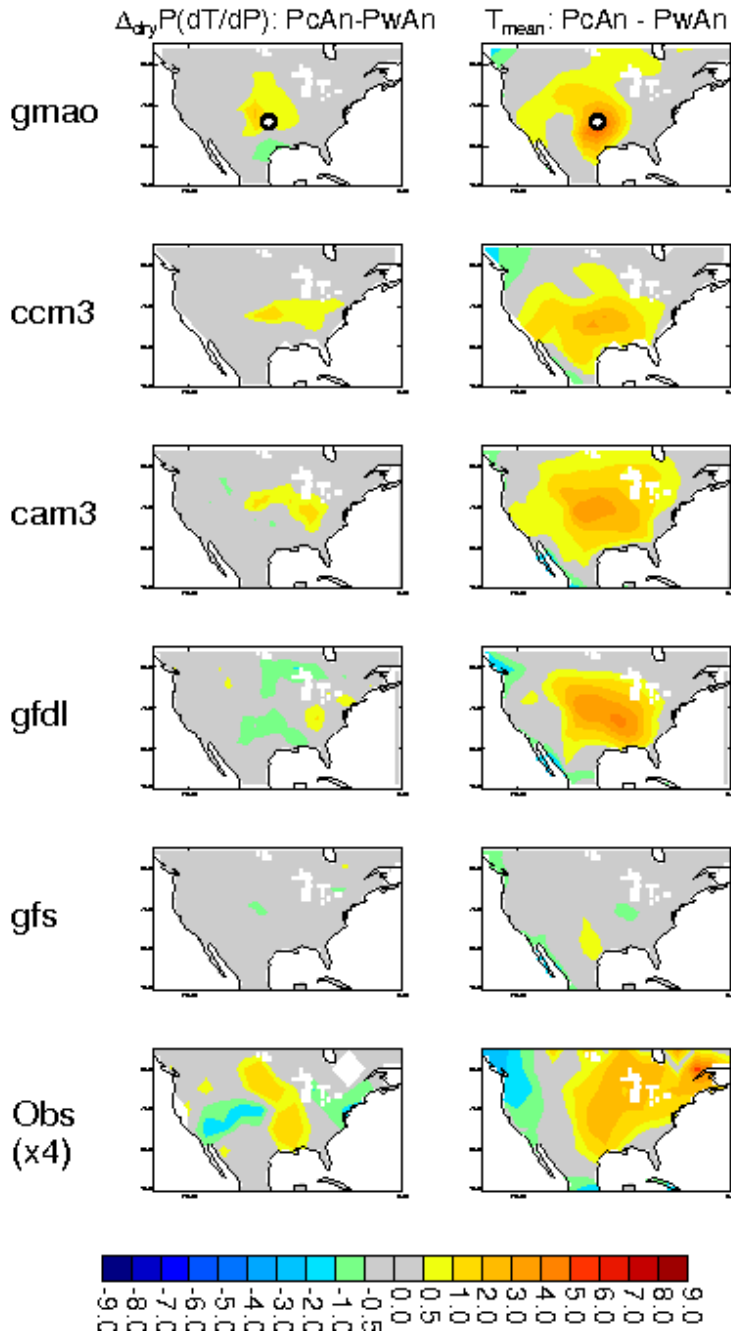


Figure 6. Relative magnitudes of the $\Delta_{\text{PcAn-PwAn}} [\Delta_{\text{dry}}P(dT/dP)]$ and $\Delta_{\text{PcAn-PwAn}} [T_{\text{mean}}]$ terms contributing to the difference $T_{\text{dry}}(\text{PcAn}) - T_{\text{dry}}(\text{PwAn})$, as outlined in equation (2). Units are $^{\circ}\text{K}$. The black circle in the top row panels locates the grid cell examined in Figures 3 and 4. Values for the observational data are multiplied by four prior to plotting, to reflect (qualitatively) the weaker SST signal examined.

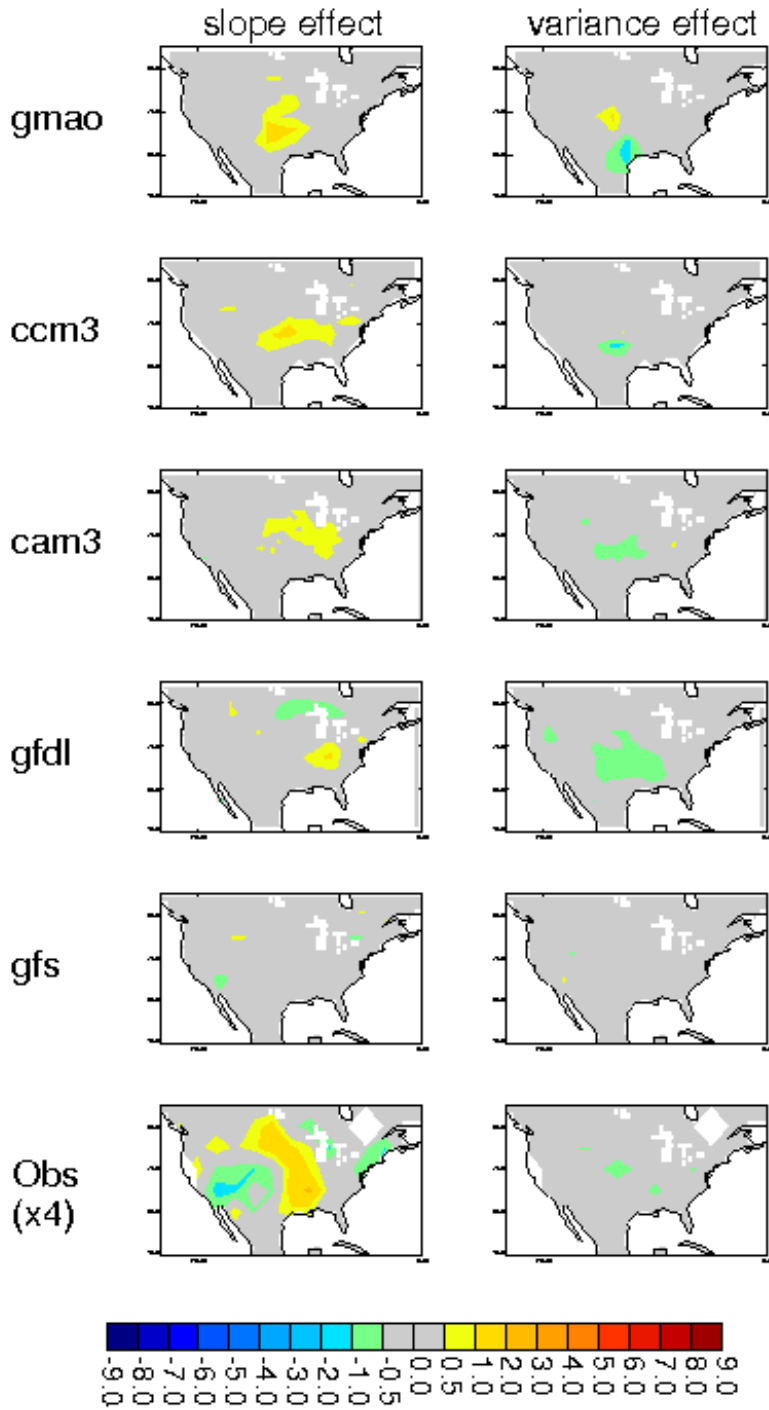


Figure 7. Relative contributions of the “temperature sensitivity” (dT/dP) and “precipitation variance” ($\Delta_{dry}P$) terms to the $\Delta_{dry}P$ (dT/dP) differences shown in Figure 6, as outlined in equation (3). Units are $^{\circ}K$. Values for the observational data are multiplied by four prior to plotting, to reflect (qualitatively) the weaker SST signal examined.

Differences from observed mean JJA temperature

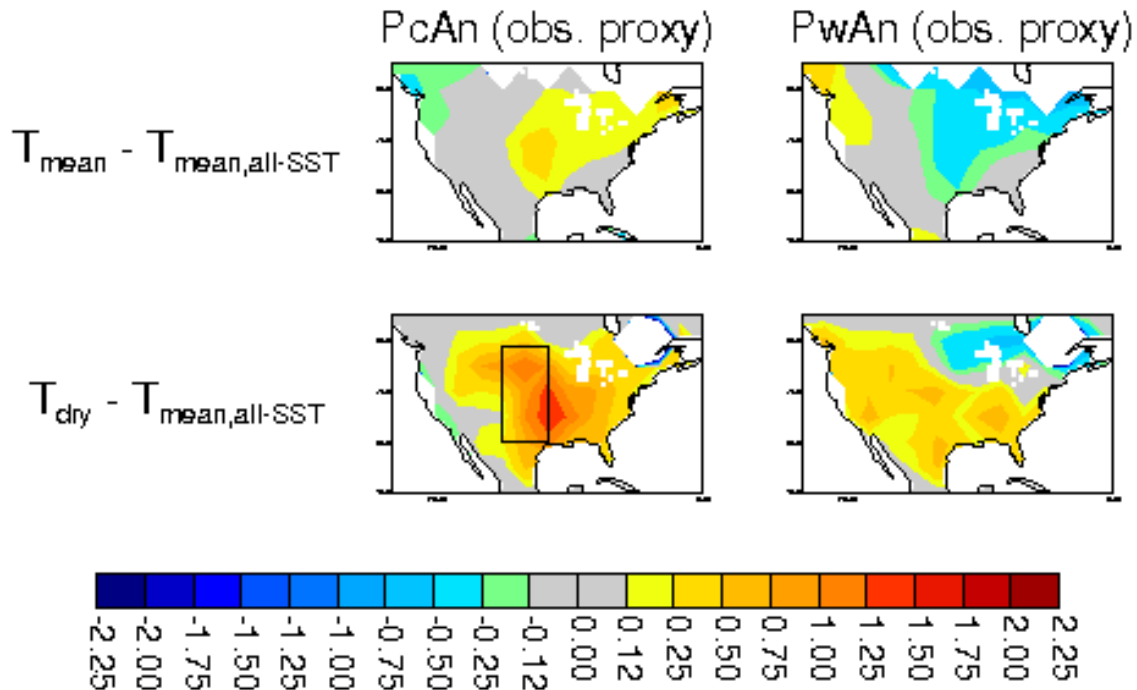


Figure 8. Top left: Values of observed T_{mean} (in $^{\circ}\text{C}$) for proxy PcAn conditions minus the long term average JJA temperature for all SST conditions. Top right: Same, but for proxy PwAn conditions. Bottom left: Values of observed T_{dry} (in $^{\circ}\text{C}$) for proxy PcAn conditions minus the long term average JJA temperature for all SST conditions. (The outlined region is examined further in Figure 9.) Bottom right: Same, but for PwAn conditions.

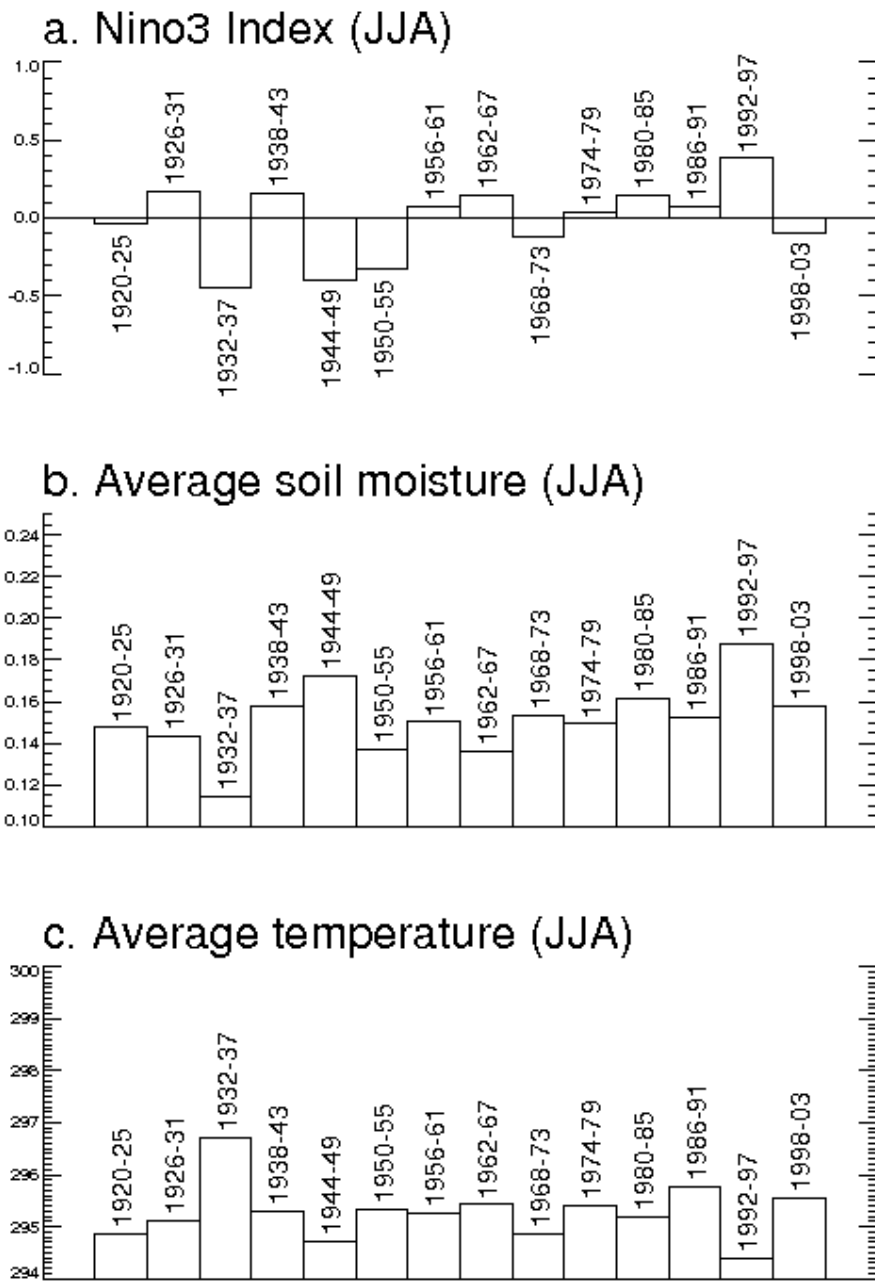


Figure 9. a. Average of Nino3 index (for JJA) over six year periods spanning 1920 to 2003. b. Corresponding average soil moisture (volumetric) in the U.S. Great Plains, as simulated in an extended offline simulation with a land surface model driven with observations-based forcing. c. Corresponding surface temperature in the U.S. Great Plains, as established through the same offline simulation.